Northumbria Research Link

Northumbria
University
NEWCASTLE

UniversityLibrary

Bending-Shear Interaction of Cold-Formed Stainless Steel Lipped Channel Sections

D. M. M. P. Dissanayake

Faculty of Engineering and Environment, University of Northumbria,

Newcastle, UK.

K. Poologanathan

Faculty of Engineering and Environment, University of Northumbria,

Newcastle, UK.

S. Gunalan

School of Engineering and Built Environment, Griffith University,

Gold Coast, Australia.

K. D. Tsavdaridis

School of Civil Engineering, Faculty of Engineering and Physical Sciences, University of

Leeds, UK.

K. S. Wanniarachchi

Faculty of Engineering, University of Ruhuna, Sri Lanka.

B. Nagaratnam

Faculty of Engineering and Environment, University of Northumbria,

Newcastle, UK.

Abstract

The bending-shear interaction response of cold-formed stainless steel lipped channel sections has been given inadequate attention in the past. Therefore, this paper investigates the bending and shear interaction behaviour of cold-formed stainless steel lipped channel sections using numerical studies. Finite element (FE) models were developed and validated against the experimental results found in the literature for three-point and four-point loading tests of lipped channel sections of both cold-formed stainless steel and cold-formed steel. The elaborated FE results were used for a comprehensive parametric study that was conducted comprising 60 FE models of three-point loading simulations of stainless steel lipped channels with five different aspect ratios to study the shear response and the bending-shear interaction response. Another 12 FE models of four-point bending simulations were developed to study the bending response.

The numerical results were analysed and it was found that the sections with aspect ratios of 1.5 and 2.0 are subjected to the interaction of bending and shear while there is no interaction effect observed in the sections with other aspect ratios. Eurocode 3 and American specifications interaction equations were then evaluated using the numerical results. These design provisions are found to be too conservative for a higher level of applied shear force. Therefore, revised design equations for bending and shear interaction were proposed aiming better prediction accuracy. Further, a statistical evaluation was conducted for the proposed interaction equations and results suggested improved and consistent predictions.

Keywords: Lipped channel beams, Cold-formed stainless steel, Bending-shear interaction, Numerical modelling, Eurocode 3, American specifications, Design rules

1   Introduction

Lipped channel beam (LCB) sections have commonly been used as load-bearing components such as roof purlins, wall studs, and floor joists in the structural applications. In practice, a higher level of stresses is developed within the cross-sections, due to the interaction of the bending and shear actions prevalent, in particular, at the supports of continuous spans and cantilever beams. The bending and shear resistances of a section tend to reduce under the bending-shear interaction, thus it is worth investigating this bending-shear interaction in the structural design process. The interaction of the bending and shear actions of hot-rolled, plate girder and cold-formed sections has been the motive for a number of investigations conducted over the years. The initial experiments on stainless steel plate girders have been performed by Olsson [1] while Real et al. [2] conducted both testing and numerical modelling of stainless steel plate girders to study the shear response. The bending-shear interaction behaviour of stainless steel plate girders have been investigated by Saliba and Gardner [3] and Chen et al. [4] using experimental and numerical studies. Sinur and Beg [5],[6] have also carried out both experimental and numerical studies on stiffened carbon steel plate girders. In addition, a number of studies have been performed on cold-formed steel sections. Keerthan and Mahendran [7] experimented the bending-shear interaction behaviour of cold-formed steel lipped channel sections, while, Pham and Hancock [8] performed both experimental and numerical studies. Furthermore, the bending-shear interaction behaviour of cold-formed steel hollow flange channel sections has been studied by Keerthan et al. [9]. However, no comprehensive investigation has been conducted for cold-formed stainless steel lipped channel

64 sections in the context of bending and shear interaction behaviour. Therefore, this gap in the

65 literature was covered in this study.

66 Most of the design provisions for bending-shear interaction have been based on the resistance

67 model first proposed by Basler [10]. Basler [10] investigated the bending-shear interaction of

68 longitudinally unstiffened plate girders with slender webs and proposed a mechanical model

69 considering the effect of interaction. This model includes the post-buckling effects of slender

70 webs and is given by Eq. (1).

71 $\left(\dfrac{V}{V_w}\right)^2 + \dfrac{M-M_f}{M_p-M_f} = 1$ for $M_f < M < M_{eff}$ (1)

72 where V_w is the web shear capacity, M_f is the bending capacity of flanges alone, M_p is the

73 plastic bending capacity of the whole section, M_{eff} is the bending capacity of the effective cross-

74 section, and V and M are the design shear force and design bending moment, respectively.

75 In this resistance model for bending-shear interaction, it is assumed that when the applied

76 bending moment is less than the flange bending resistance, the applied bending moment is

77 resisted solely by the flanges, therefore, no reduction occurs in the shear capacity of the webs.

78 However, when the sections are subjected to higher moments than the flange bending

79 resistance, a part of the section moment is transferred to the section webs and therefore, the

80 web shear resistance begins to reduce. Thus, the interaction of bending and shear actions has

81 to be considered.

82 In the current version of European standards for stainless steel (EN1993-1-4 [11]), no

83 provisions have been made for the bending and shear interaction. This is because, EN1993-1-

84 4 [11] provides only the supplementary provisions for stainless steel and therefore, European

85 standards for cold-formed steel (EN1993-1-3 [12]) and European standards for plated steel

86 (EN1993-1-5 [13]) are to be referred for the bending and shear interaction design of stainless

87 steel cold-formed and plated sections, respectively. These interaction provisions are based on

88 a modified version of Basler's [10] resistance model.

89 Bleich [14] has investigated the bending-shear interaction response of rectangular plates and

90 proposed a circular interaction equation. This is expressed in Eq. (2). This was found to be

91 conservative for sections with transverse stiffeners. Therefore, Shahabian and Roberts [15]

92 have suggested a rounded interaction equation and is given by Eq. (3). Moreover, LaBoube and

93   Yu [16] have conducted experiments on the bending-shear interaction behaviour of cold-
94   formed steel lipped channel sections without transverse stiffeners. Based on their work,
95   LaBoube and Yu [16] have also proposed a relationship for the bending-shear interaction.
96   Modified versions of some of these interaction equations have been the basis for the bending
97   and shear interaction design provisions in American specifications for cold-formed stainless
98   steel design, SEI/ASCE 8–02 [17].

99   $$\left(\frac{M}{M_n}\right)^2 + \left(\frac{V}{V_n}\right)^2 \leq 1.0 \tag{2}$$

100 $$\left(\frac{M}{M_n}\right)^4 + \left(\frac{V}{V_n}\right)^4 \leq 1.0 \tag{3}$$

101 where M_n and V_n are nominal bending strength and nominal shear strength of the section,
102 respectively.

103 This paper presents the details of numerical investigations carried out to study the bending-
104 shear interaction behaviour of cold-formed stainless steel lipped channel sections. First, a
105 summary of codified design provisions for bending-shear interaction is discussed. Then, the
106 details of developing the finite element (FE) models and the validation study are outlined.
107 Thereafter, the results of the comprehensive parametric study conducted are presented. Finally,
108 the analysis of numerical results, assessment of available design provisions, and suggested
109 modifications to them in the context of bending-shear interaction of stainless steel LCBs are
110 elaborated.

111 **2   Review of design rules**

112 In this section, design provisions for bending and shear interaction found in European standards
113 and American specifications are discussed.

114 2.1   Eurocode 3 design provisions

115 In the absence of provisions for bending and shear interaction, European standards for stainless
116 steel (EN1993-1-4 [11]) refers to the provisions given in European standards for cold-formed
117 steel (EN1993-1-3 [12]) for the bending-shear interaction design of stainless steel cold-formed
118 sections. Interaction equation provided in EN1993-1-3 [12] is based on Basler's [10] resistance
119 model and is given by Eq. (4). This interaction model is valid only when the applied shear force
120 (V_{Ed}) is greater than 50 % of the web shear resistance ($V_{w,Rd}$) and when the applied moment

121   ($M_{y,Ed}$) exceeds the bending resistance corresponding to the effective areas of flanges alone

122   ($M_{f,Rd}$).

123    $$\frac{M_{y,Ed}}{M_{y,Rd}} + \left(1 - \frac{M_{f,Rd}}{M_{pl,Rd}}\right)\left(\frac{2V_{Ed}}{V_{w,Rd}} - 1\right)^2 \leq 1.0 \tag{4}$$

124   where $M_{y,Rd}$ is the bending resistance and $M_{pl,Rd}$ is the plastic bending resistance of the section.

125   For the calculation of bending resistance consisting of the effective flange area ($M_{f,Rd}$) and the

126   plastic bending resistance of the section ($M_{pl,Rd}$), provisions given in EN1993-1-5 [13] should

127   be referred. This includes the calculation of the effective widths of plate elements according to

128   the effective width method to account for the loss of effectiveness due to the local buckling.

129   The cross-section bending resistance ($M_{y,Rd}$) can be calculated using Eq. (5) based on effective

130   cross-section properties according to EN1993-1-4 [11].

131    $$M_{y,Rd} = M_{eff,Rd} = \frac{W_{y,eff}f_y}{\gamma_{M0}} \tag{5}$$

132   where $W_{y,eff}$ is the effective section modulus, f_y is the yield strength, and γ_{M0} is the partial factor

133   for cross section resistance.

134   The rotated stress field theory proposed by Höglund [18] has been adopted in European

135   standards for stainless steel (EN1993-1-4 [11]) to calculate section shear resistance. However,

136   for the bending-shear interaction calculation, only the web contribution to shear resistance

137   ($V_{w,Rd}$) is considered and this is given by Eq. (6).

138    $$V_{w,Rd} = \frac{\chi_w f_{yw} h_w t_w}{\sqrt{3}\gamma_{M1}} \tag{6}$$

139   where χ_w is the web shear buckling reduction factor which is a function of web slenderness

140   ($\bar{\lambda}_w$), f_{yw} is the yield strength, h_w is the web height, t_w is the web thickness, and γ_{M1} is the

141   partial factor for member resistance. Table 1 gives the set of equations provided in EN1993-1-

142   4 [11] for the web shear buckling reduction factor (χ_w) of the sections with rigid end posts.

143   Dissanayake et al. [19] has modified this set of expressions for web shear buckling reduction

144   factor (χ_w) considering cold-formed stainless steel lipped channel sections and those are given

145   in Table 2.

146

147 Table 1 Web shear buckling reduction factor (χ_w) of EN1993-1-4 [11] for the sections with rigid end post.

	χ_w
$\bar{\lambda}_w \leq 0.65/\eta$	η
$0.65/\eta < \bar{\lambda}_w < 0.65$	$0.65/\bar{\lambda}_w$
$\bar{\lambda}_w \geq 0.65$	$1.56/(0.91 + \bar{\lambda}_w)$

148

149 Table 2 Proposed expressions of web shear buckling reduction factor (χ_w) for the sections with rigid end post by
150 Dissanayake et al. [19].

	χ_w
$\bar{\lambda}_w \leq 0.12$	2.1
$0.12 < \bar{\lambda}_w < 0.667$	$0.839/\bar{\lambda}_w^{0.433}$
$\bar{\lambda}_w \geq 0.667$	$1.797/(1.13 + \bar{\lambda}_w)$

151

152 ## 2.2   American specifications, SEI/ASCE 8–02

153 In American specifications for cold-formed stainless steel (SEI/ASCE 8–02 [17]), two separate
154 equations have been provided for the bending-shear interaction, which are for sections with
155 and without transverse stiffeners. From Eq. (7), SEI/ASCE 8–02 [17] provision for sections
156 with transverse stiffeners is given and this takes into account the bending-shear interaction
157 when the applied bending moment (M) exceeds half of the section nominal moment capacity
158 (M_n) and when the applied shear force (V) is greater than 70 % of the section nominal shear
159 capacity (V_n).

160 $$0.6 \left(\frac{M}{M_n}\right) + \left(\frac{V}{V_n}\right) \leq 1.3 \text{ for } \frac{M}{M_n} > 0.5 \text{ and } \frac{V}{V_n} > 0.7 \qquad (7)$$

161 For the calculation of nominal capacities, the direct strength method (DSM) can be
162 incorporated. The nominal bending strength for local buckling (M_{nl}) from AISI S100 [20] can
163 be used to determine the nominal bending strength (M_n) and is expressed in Eqs. (8) and (9).

164 $$M_{nl} = M_{ne} \text{ for } \lambda_l \leq 0.776 \qquad (8)$$

6

165 $$M_{nl} = \left[1 - 0.15 \left(\frac{M_{crl}}{M_{ne}}\right)^{0.4}\right] \left(\frac{M_{crl}}{M_{ne}}\right)^{0.4} M_{ne} \text{ for } \lambda_l > 0.776 \tag{9}$$

166 where M_{ne} is the critical elastic lateral-torsional buckling moment, M_{crl} is the critical elastic

167 local buckling moment, and λ_l is the section slenderness.

168 The nominal shear strength (V_n) can be calculated from AISI S100 [20] using Eqs. (10) and

169 (11).

170 $$V_n = V_y \text{ for } \lambda_v \leq 0.776 \tag{10}$$

171 $$V_n = \left[1 - 0.15 \left(\frac{V_{cr}}{V_y}\right)^{0.4}\right] \left(\frac{V_{cr}}{V_y}\right)^{0.4} V_y \text{ for } \lambda_v > 0.776 \tag{11}$$

172 where V_y is the shear yield force, V_{cr} is the elastic shear buckling force, and λ_v is the section

173 slenderness.

174 Dissanayake et al. [19] also proposed modified set of equations to determine the shear strength

175 of cold-formed stainless steel lipped channel sections using DSM and these DSM provisions

176 are expressed in Eqs. (12)-(14).

177 $$V_n = 2V_y \text{ for } \lambda_v \leq 0.122 \tag{12}$$

178 $$V_n = \frac{0.795}{\lambda_v^{0.439}} V_y \text{ for } 0.122 < \lambda_v \leq 0.592 \tag{13}$$

179 $$V_n = \left[1 - 0.213 \left(\frac{V_{cr}}{V_y}\right)^{0.35}\right] \left(\frac{V_{cr}}{V_y}\right)^{0.35} V_y \text{ for } \lambda_v > 0.592 \tag{14}$$

180 In addition to this linear interaction equation, a circular interaction equation is also provided in

181 SEI/ASCE 8–02 [17] for sections without transverse stiffeners and this is similar to the

182 expression given in Eq. (2).

183 **3   Finite element (FE) modelling**

184 Commercially available ABAQUS CAE 2017 software package was employed to develop the

185 FE models to investigate the bending and shear interaction behaviour of cold-formed stainless

186 steel lipped channel sections. The details of numerical simulations carried out are similar to the

187 numerical modelling out lined in Dissanayake et al. [19] and are summarised in this section.

3.1   General

189   Three-point loading tests of LCBs found from [7],[19] were simulated in ABAQUS to study

190   the bending-shear interaction. To avoid any torsional effects on the structural behaviour of

191   LCBs, back-to-back beam setup has been employed by attaching two LCBs from their webs in

192   the experiments. Simply supported boundary conditions and mid-span loading have been

193   assigned to the sections through hot-rolled T-stiffeners. The T-stiffeners have been bolted to

194   two LCBs using web side plates to avoid any web bearing failure. Both top and bottom flanges

195   have been restrained against distortional buckling by screwing equal angle (EA) straps to them

196   at the loading point and at two supports. More details of these three-point loading tests can be

197   found in [7],[19],[21]–[23]. However, considering the symmetry of the test setup, single LCBs

198   were simulated with three web side plates in the FE models developed in this study. The

199   schematic diagram of three-point loading test setup and cross-sectional dimensions of a LCB

200   section are shown in Fig. 1. In the FE modelling, the shear behaviour and the bending-shear

201   interaction behaviour of LCBs were simulated using this setup.

202   In addition, it was required to study the bending behaviour of LCBs to find out their bending

203   capacities. For this purpose, four-point bending test setup given in [8] was utilised and then FE

204   models were developed for each cross-section considered in this study. More details of four-

205   point bending tests can be found in [8],[24].
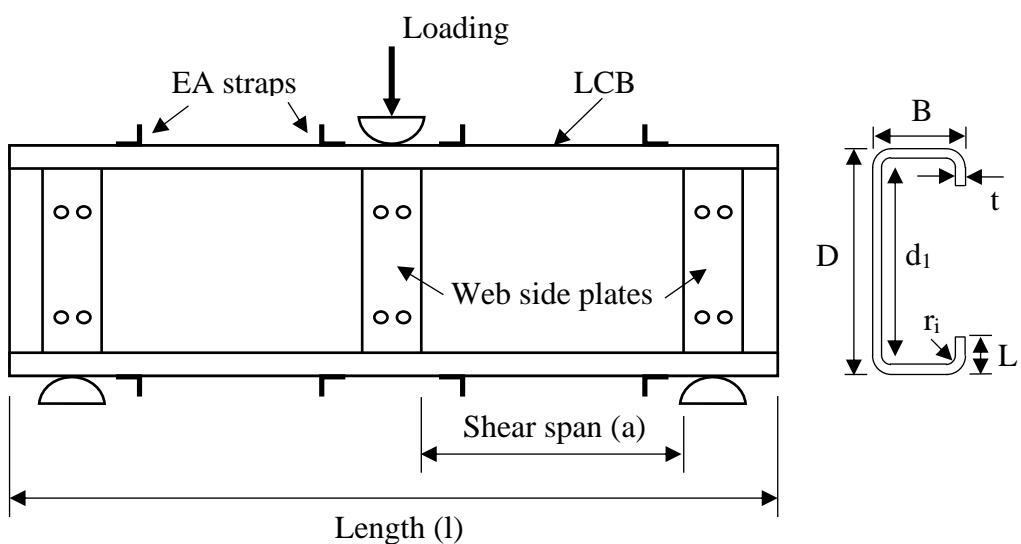
206

207   Fig. 1 Schematic diagram of three-point loading arrangement and cross-sectional dimensions

208   3.2   Element type and mesh

209   The four-node shell element type known as S4R was chosen from ABAQUS element library

210   to model both LCB sections and web side plates. These S4R shell elements have six degrees

211   of freedom (DOFs) at each node. Mesh sensitivity analysis suggested that the assigning of 5

212   mm × 5 mm mesh for flat parts of LCB sections and assigning of a relatively finer mesh of 1

213   mm × 5 mm for corner regions of LCB sections are sufficient. However, as web side plates are

214   less important, a comparatively coarser mesh of 10 mm × 10 mm was used for modelling them.

215   Fig. 2 illustrates the assembly of parts together with the FE mesh assigned in the modelling.

(a)

(b)
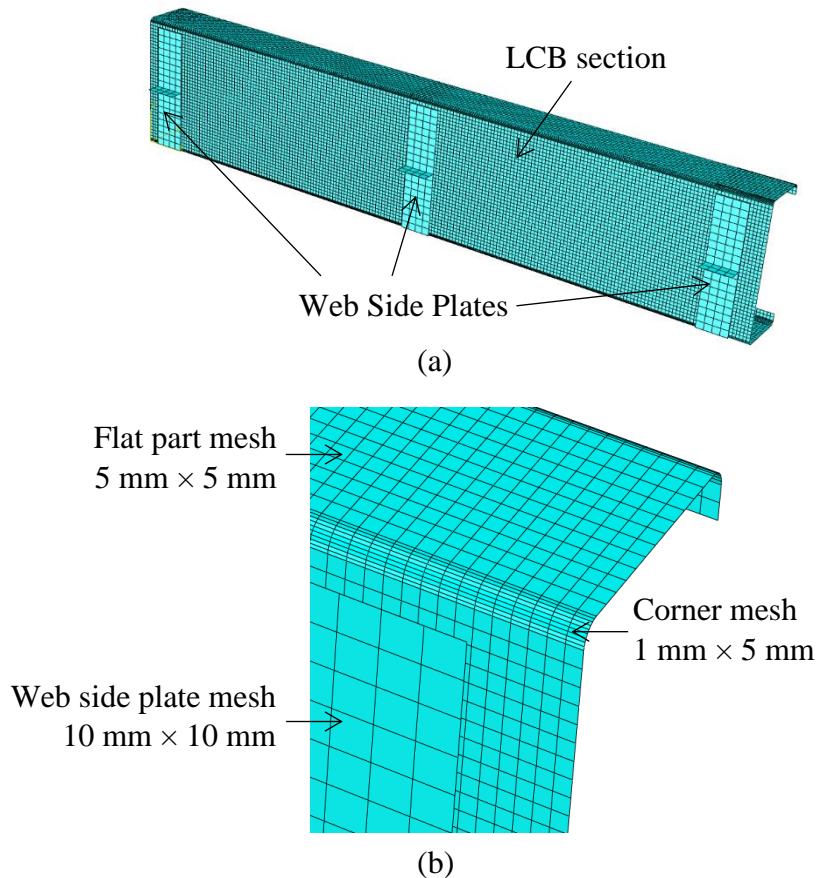
216

217   Fig. 2 (a) Assembly of parts and (b) FE mesh used in the modelling

218   3.3   Material modelling of stainless steel

219   Arrayago et al. [25] have recently proposed modifications to the two-stage Ramberg-Osgood

220   material model. The modified two-stage Ramberg-Osgood material model with these recent

221   proposals was incorporated in calculating stress-strain data for stainless steel in this study.

222   Then, true stress (σ_{true}) and log plastic strain (ε_{ln}^{pl}) data of the non-linear material was inputted

223   into ABAQUS. The true stress (σ_{true}) and log plastic strain (ε_{ln}^{pl}) were calculated using Eqs.

224   (15) and (16), respectively. The strength enhancements induced during the press-braking

225   process of LCB sections were introduced to the corner regions as described in [19]. For the FE

226   modelling of carbon steel sections, an elastic, perfectly-plastic material model was employed.

227   The incorporated material models are illustrated in Fig. 3.

228     $$\sigma_{true} = \sigma_{nom}(1 + \varepsilon_{nom}) \qquad (15)$$

229     $$\varepsilon_{ln}^{pl} = \ln(1 + \varepsilon_{nom}) - \frac{\sigma_{true}}{E} \qquad (16)$$

230   where σ_{nom} is the engineering stress, ε_{nom} is the engineering strain, and E is Young's

231   modulus.
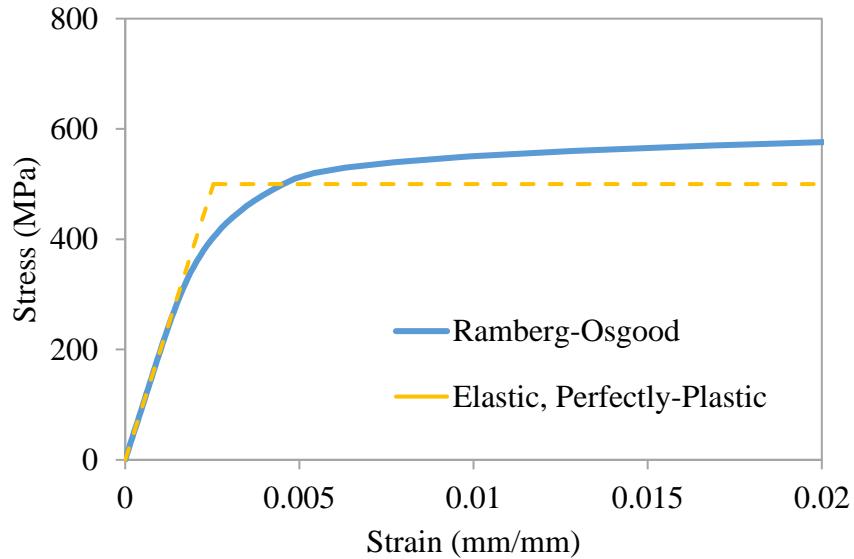
232

233   Fig. 3 Different material models used in the FE modelling

234   During the section forming, two types of residual stresses are formed in press-braked sections

235   and these are known as bending and membrane residual stresses. The bending residual stresses

236   are indirectly accounted in material stress-strain data while membrane residual stresses are

237   found to be negligible for press-braked sections [26]. The similar numerical studies have also

238   ignored the residual stresses arising from the section forming in the numerical modelling as

239   these residual stresses have very small effect [26],[27]. Therefore, the effect of these residual

240   stresses were not explicitly considered in the FE modelling of this study.

241   3.4   Boundary conditions

242   The boundary conditions were chosen as they accurately simulate the experimental conditions.

243   All three translational DOFs were restrained at one end to maintain a pin support condition

244   while only the translational DOFs in the cross-sectional plane were restrained at the other end

245   to maintain a roller support condition. To avoid any rotation of the section, the rotational DOF

246   about the longitudinal axis was restrained at both supports. The loading was given at the mid-

247   span by applying a vertical displacement. The loading and the support conditions were assigned

248   to web side plates to suppress any web bearing failure at these locations. The translational DOF

249   in the transverse direction and the rotational DOF about the longitudinal axis were restrained

250   at the EA strap locations to eliminate distortional buckling. To simulate bolted connections

251   between LCB web and web side plates, tie constraints (available in ABAQUS) were assigned.

252   The locations of the assigned boundary conditions in the FE modelling are given in Fig. 4.
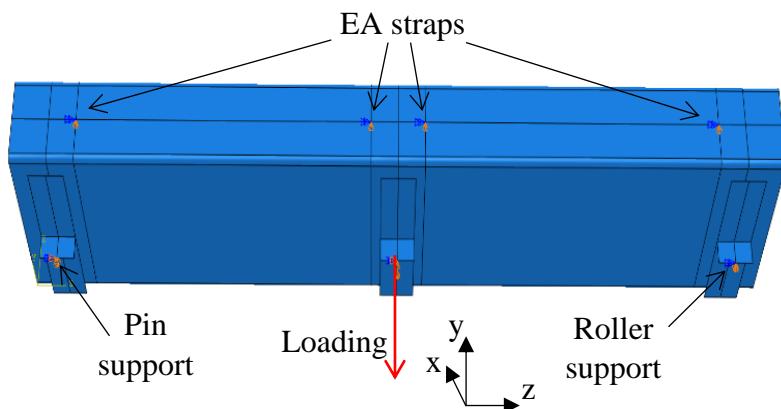
253

254   Fig. 4 The locations of the boundary conditions assigned in the FE modelling

255   3.5   Analysis methods

256   To account for geometric imperfections in the non-linear analysis, first, an Eigenvalue buckling

257   analysis was conducted on the perfect geometry. Then, the critical buckling Eigenmode shapes

258   were extracted from the analysis. The web shear buckling mode with the lowest Eigenvalue

259   was chosen from each analysis. Thereafter, these critical mode shapes were superimposed on

260   to the non-linear FE models using a suitable scale factor which represents the magnitude of

261   imperfections. In this study, the modified Dawson and Walker model proposed by Gardner and

262   Nethercot [28] was used as the imperfection amplitude (ω_0). The modified Dawson and

263   Walker model is given by Eq. (17).

11

264 $$\omega_0 = 0.023 \left(\frac{\sigma_{0.2}}{\sigma_{cr}}\right) t \qquad\qquad (17)$$

265 where $\sigma_{0.2}$ is the 0.2 % proof stress of the material, σ_{cr} is the critical elastic buckling stress of

266 the most slender element of the section, and t is the thickness.

267 Secondly, a modified static Riks analysis was performed on the geometrically and materially

268 non-linear FE models until the failure occurs, to study the section behaviour. More details

269 related to FE modelling of cold-formed channel sections can be found from [29]–[31].

4 Validation of FE models

271 Comparisons of the FE results obtained from the developed models were compared with the

272 experimental results found from the literature and those details are given in this section. The

273 shear, bending, and bending-shear interaction tests were covered in this validation process.

274 In this paper, LCB cross-sections are denoted as LCB D × B × L × t. This notation stands for

275 key cross-sectional dimensions in millimetres where D is the section depth, B is the flange

276 width, L is the lip height, and t is the section thickness. These cross-sectional dimensions are

277 defined in Fig. 1.

278 4.1 Shear behaviour

279 Dissanayake et al. [19] have investigated the shear behaviour of cold-formed stainless steel

280 LCBs using three-point loading tests. These experimental results are compared with the FE

281 results in Table 3 for the validation of FE modelling for shear behaviour. The section length

282 and the shear span length for each section are also given in Table 3. The shear span (a) to clear

283 web depth (d_1) ratio is taken as the aspect ratio of the specimen and the definition of these

284 parameters are illustrated in Fig.1. The shear capacity of a section is independent of its bending

285 stresses when shorter spans (such as sections with an aspect ratio of 1.0) are employed while

286 the bending-shear interaction is taken place when longer spans are employed [7]. Therefore,

287 all the compared sections have an aspect ratio of 1.0. From the comparisons, it can be seen that

288 the mean and the coefficient of variation (COV) of experimental to FE shear capacity ratio are

289 1.02 and 0.073, respectively. This confirms the ability of developed FE models to predict the

290 shear capacities of cold-formed stainless steel LCBs with good accuracy. Additionally, Fig. 5

291 compares the experimental and FE shear failure modes for LCB 200×75×15×1.2 section. It can

292 be concluded from Fig. 5, that the developed FE models are able to accurately capture the

diagonal shear failures of LCB webs as well. The experimental and FE load-deflection curves of LCB 150×65×15×2.0 section are also compared in Fig. 6. The slip between the plates and specimens at the bolted connections could be the reason for higher deflections in the experiments compared to FE results.

Table 3 Comparison of experimental [19] and FE section capacities for stainless steel LCBs subjected to shear

LCB section	l (mm)	a (mm)	$\bar{\lambda}_w$	$V_{Exp.}$ (kN)	V_{FE} (kN)	$\dfrac{V_{Exp.}}{V_{FE}}$
LCB 100×50×15×1.2	380	97.5	0.78	18.49	16.86	1.10
LCB 100×50×15×1.5	379	97.0	0.61	24.44	23.90	1.02
LCB 100×50×15×2.0	376	95.5	0.45	36.00	32.72	1.10
LCB 150×65×15×1.2	479	147.0	1.17	21.60	20.09	1.08
LCB 150×65×15×1.5	479	147.0	0.92	26.26	28.40	0.92
LCB 150×65×15×2.0	478	146.5	0.69	43.55	42.60	1.02
LCB 200×75×15×1.2	579	197.0	1.57	22.98	22.97	1.00
LCB 200×75×15×2.0	579	197.0	0.93	47.05	52.11	0.90
Mean						1.02
COV						0.073

(a)　　　　Shear failure　　　　(b)
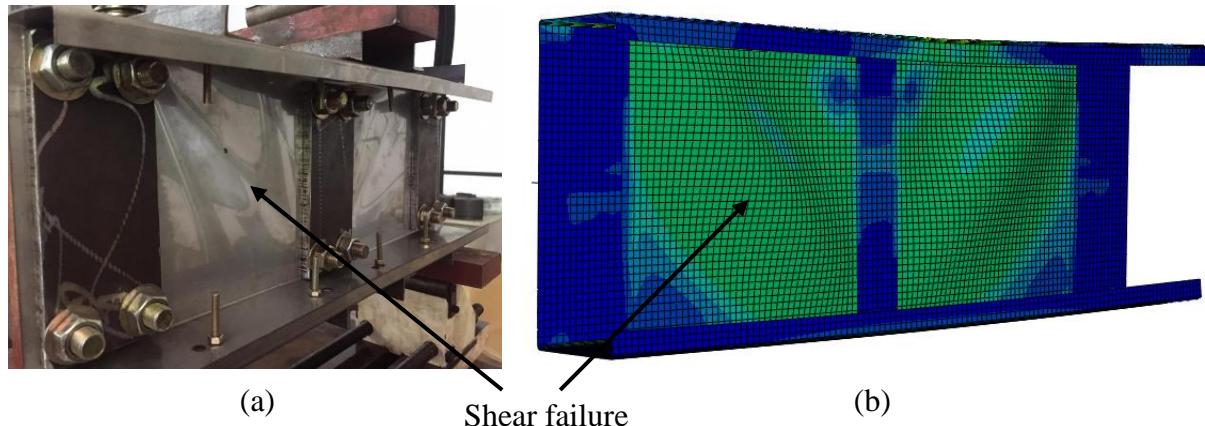
Fig. 5 (a) Experimental [19] and (b) FE failure modes of stainless steel LCB 200×75×15×1.2 section subjected to shear
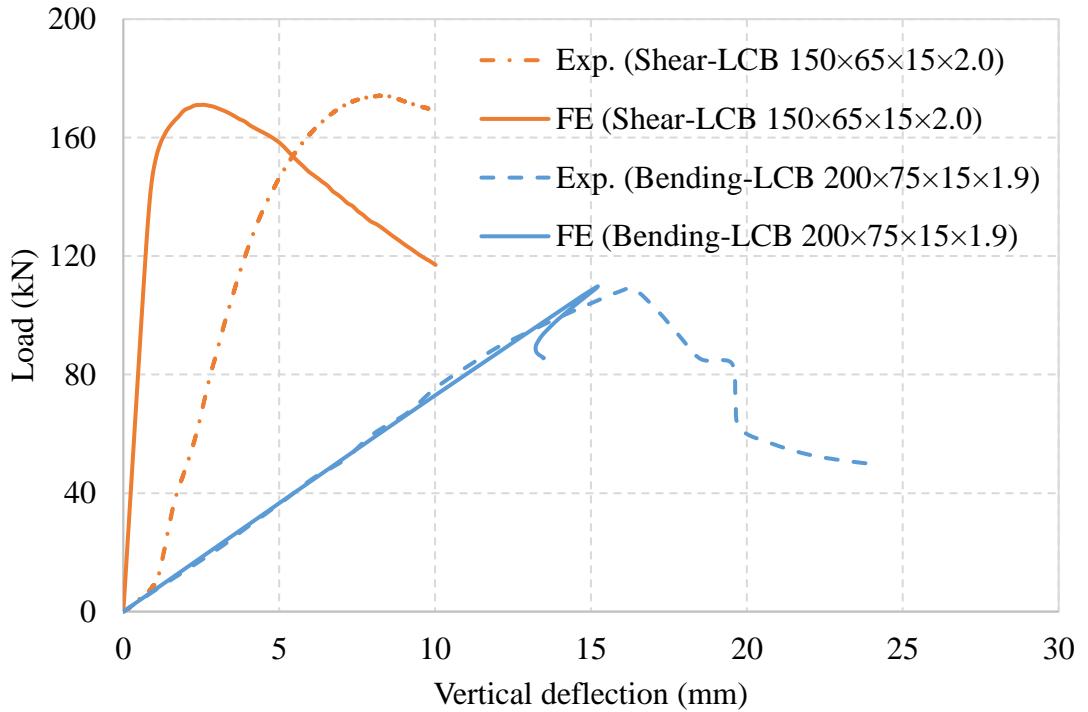
Fig. 6 Comparison of experimental and FE load-deflection curves

4.2 Bending behaviour

To study the bending behaviour, four-point bending tests of cold-formed steel LCB sections found from Pham and Hancock [8] were simulated in ABAQUS. A specimen length of 2695 mm was utilised in the FE modelling according to bending tests conducted by Pham and Hancock [8]. In the FE modelling, an elastic, perfectly-plastic material model was employed for cold-formed steel, with no consideration given to corner strength enhancements. Experimental and FE ultimate loads of four-point bending tests of cold-formed steel LCB sections are compared in Table 4. In Table 4, P is the ultimate load. The experimental to FE ultimate load ratio has a mean and a COV of 1.02 and 0.056, respectively. Therefore, good accuracy of capacity predictions is evident from the comparisons. In addition, comparisons are made between experimental and FE failure modes in Fig. 7 and experimental and FE load-deflection curves in Fig. 6 for LCB 200×75×15×1.9 section. Both these comparisons show good agreement as well. Therefore, the elaborated FE models can be utilised to study the bending response of cold-formed stainless steel LCB sections.

Table 4 Comparison of experimental [8] and FE section capacities for cold-formed steel LCBs subjected to bending

LCB section	$P_{Exp.}$ (kN)	$M_{Exp.}$ (kNm)	P_{FE} (kN)	M_{FE} (kNm)	$\dfrac{P_{Exp.}}{P_{FE}}$
LCB 150×65×15×1.5	52.13	10.43	53.64	10.73	0.97
LCB 150×65×15×2.4	99.19	19.84	90.04	18.01	1.10
LCB 200×75×15×1.5	67.33	13.47	66.00	13.20	1.02
LCB 200×75×15×1.9	108.78	21.76	109.80	21.96	0.99
Mean					1.02
COV					0.056

(a)

Bending failure

(b)
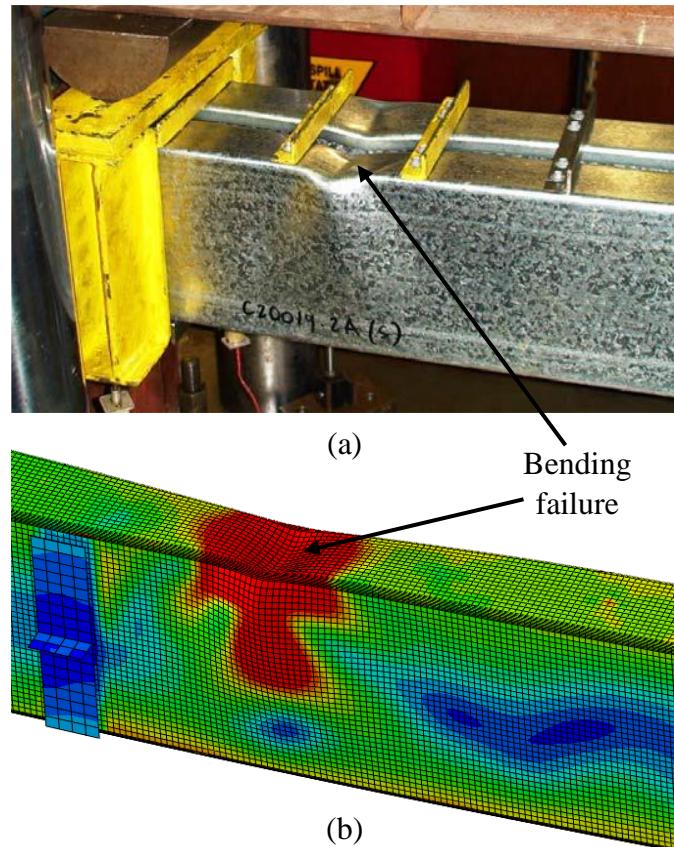
Fig. 7 (a) Experimental [8] and (b) FE failure modes of cold-formed steel LCB 200×75×15×1.9 section subjected to bending

325   4.3   Bending-shear interaction behaviour

326   Keerthan and Mahendran [7] have investigated the bending-shear interaction behaviour of

327   cold-formed steel LCB sections with an aspect ratio (a/d_1) of 1.5 using three-point loading tests.

328   These tests were simulated in the FE modelling and results were compared. Table 5 summarises

329   the experimental and FE capacities. From the comparisons, it can be seen that the experimental

330   to FE shear capacity ratio has a mean of 1.01 and a COV of 0.067. Therefore, the capacity

331   prediction accuracy of the FE models is highlighted for higher aspect ratios as well. Moreover,

332   good agreement can be seen between experimental and FE bending-shear interaction failure

333   modes for LCB 250×75×18×1.9 section in Fig. 8.

334   Table 5 Comparison of experimental [7] and FE section capacities for cold-formed steel LCBs subjected to

335   bending-shear interaction

LCB section	l (mm)	a (mm)	$\bar{\lambda}_w$	$V_{Exp.}$ (kN)	$M_{Exp.}$ (kNm)	V_{FE} (kN)	M_{FE} (kNm)	$\dfrac{V_{Exp.}}{V_{FE}}$ or $\dfrac{M_{Exp.}}{M_{FE}}$
LCB 160×65×15×1.5	654	156.4	1.61	39.70	9.31	38.77	9.10	1.02
LCB 160×65×15×1.9	659	158.0	1.26	56.80	13.46	53.50	12.68	1.06
LCB 200×75×15×1.5	775	196.8	2.05	38.10	11.25	41.30	12.19	0.92
LCB 200×75×15×1.9	776	197.0	1.58	56.91	16.82	58.77	17.37	0.97
LCB 200×75×15×1.95	776	197.0	1.12	39.51	11.68	36.38	10.75	1.09
LCB 250×75×18×1.5	927	247.2	2.56	42.90	15.91	44.50	16.50	0.96
LCB 250×75×18×1.9	927	247.3	1.98	60.70	22.52	64.28	23.84	0.94
LCB 250×75×18×1.95	929	248.0	1.41	44.37	16.51	40.55	15.08	1.09
Mean								1.01
COV								0.067

336

(a)

(b)
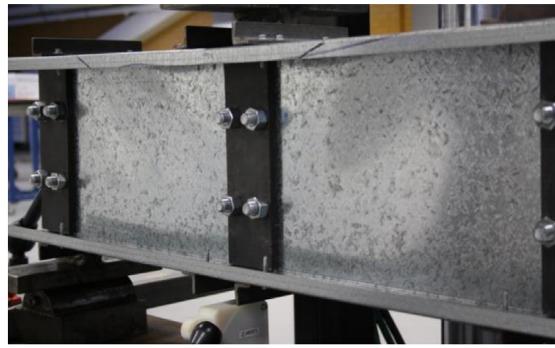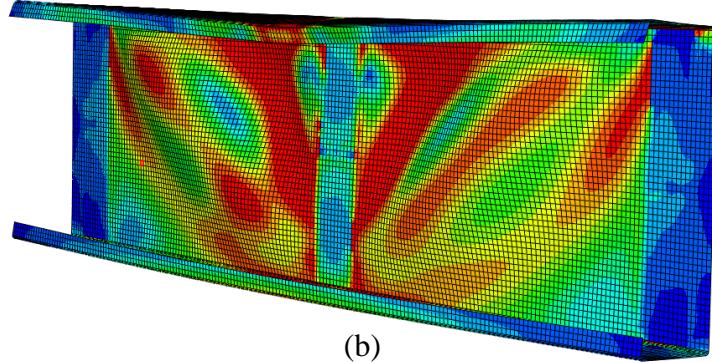
Fig. 8 (a) Experimental [7] and (b) FE failure modes of cold-formed steel LCB 250×75×18×1.9 section subjected to bending-shear interaction

5 Numerical parametric study

5.1 General

A comprehensive parametric study was conducted to generate a numerical database covering a wider area of different parameters following the successful validation of developed FE models. Then, this numerical data was utilised to investigate the bending and shear interaction behaviour of cold-formed stainless steel LCBs.

Three scenarios were considered in the study. The validated FE models of three-point loading tests with shorter spans (in Section 4.1) were utilised to simulate the shear behaviour while the validated FE models of three-point loading tests with longer spans (in Section 4.3) were considered to simulate the bending-shear interaction behaviour. In addition, the validated FE models of four-point bending tests (in Section 4.2) were incorporated to simulate the bending behaviour and to find out the bending capacities of varying LCB sections considered in the parametric study. Altogether 12 different cross sections were considered with two section depths (D), three section thicknesses (t) and two stainless steel grades. To vary the level of

17

354   bending-shear interaction, a total of 48 FE models were developed with four different aspect

355   ratio (a/d_1) values. Table 6 summarises these parameters used in the study.

356   Table 6 Summary of the parameters considered in the study

Scenario	Sections	a/d_1	l (mm)	t (mm)	Stainless steel grade	No. of models
1. Four-point bending simulation	LCB 150×65×15×t LCB 200×75×20×t	-	2695	1 1.5 2	Austenitic-1.4301 Duplex-1.4462	12
2. Three-point loading simulation with shorter spans	LCB 150×65×15×t	1	485	1	Austenitic-1.4301 Duplex-1.4462	12
	LCB 200×75×20×t	1	585	1.5 2		
3. Three-point loading simulation with longer spans	LCB 150×65×15×t	1.5	635	1	Austenitic-1.4301 Duplex-1.4462	48
		2	785	1.5		
		3	1085	2		
		5	1685			
	LCB 200×75×20×t	1.5	785			
		2	985			
		3	1385			
		5	2185			

357

358   Both austenitic and duplex stainless steel grades were considered in the study and Table 7 brief

359   the basic material properties employed in the FE models where f_y is the yield stress, f_u is the

360   ultimate stress, ε_u is the ultimate strain, and n and m are Ramberg-Osgood parameters. The

361   yield stress (f_y) and the ultimate stress (f_u) values for each stainless steel grade were taken from

362   EN1993-1-4 [11] and the recommendations of Arrayago et al. [25] were adopted for the

363   ultimate strain (ε_u) and Ramberg-Osgood parameters. Young's modulus was taken as 200,000

364   MPa and a value of 0.3 was used for Poisson's ratio. The stress-strain relationships of two

365   stainless steel grades considered are illustrated in Fig. 9.

366

367

368

369 Table 7 Material properties used in the parametric study

Stainless steel grade	f_y (MPa)	f_u (MPa)	ε_u	n	m
Austenitic-1.4301	230	540	0.57	7	2.19
Duplex-1.4462	500	700	0.29	8	3.00

370
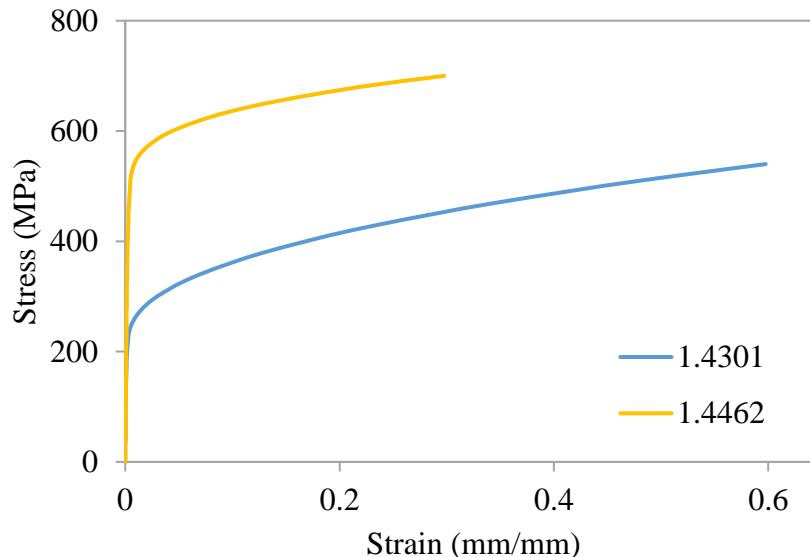
371

372 Fig. 9 Stress-strain curves for 1.4301 and 1.4462 stainless steel grades

373 5.2   Comparison of FE results with Eurocode 3 and the DSM predictions

374 The numerical parametric study results are summarised in this section. Table 8 compares the

375 cross-sectional bending capacities ($M_{u,FE}$) found from the FE simulations of four-point bending

376 setup (Scenario 1 in Table 6) with the Eurocode 3 predictions of moment resistance (M_{EC3}) and

377 the DSM predictions of moment capacity (M_{DSM}). In Table 8, M_{EC3} was calculated from Eq.

378 (5) while M_{DSM} was evaluated from Eqs. (8) and (9). From the mean and the COV of FE to

379 predicted capacity ratio, it can be concluded that the code predictions are too conservative for

380 cold-formed stainless steel LCBs. Therefore, the numerical values of cross-section bending

381 resistance ($M_{u,FE}$) were adopted in the evaluation of bending-shear interaction equations in

382 Section 6.

383

384

385

386   Table 8 Numerical parametric study results of Scenario 1

LCB section	$M_{u,FE}$ (kNm)	M_{EC3} (kNm)	M_{DSM} (kNm)	$\dfrac{M_{u,FE}}{M_{EC3}}$	$\dfrac{M_{u,FE}}{M_{DSM}}$
Stainless steel grade 1.4301					
LCB 150×65×15×1.0	3.06	2.34	2.73	1.30	1.12
LCB 150×65×15×1.5	5.75	4.55	4.95	1.26	1.16
LCB 150×65×15×2.0	8.05	6.43	6.48	1.25	1.24
LCB 200×75×20×1.0	4.30	3.33	3.85	1.29	1.11
LCB 200×75×20×1.5	8.72	6.60	7.50	1.32	1.16
LCB 200×75×20×2.0	12.80	10.41	10.72	1.23	1.19
Stainless steel grade 1.4462					
LCB 150×65×15×1.0	4.98	3.81	4.54	1.31	1.10
LCB 150×65×15×1.5	10.06	7.64	8.86	1.32	1.14
LCB 150×65×15×2.0	15.24	12.20	13.99	1.25	1.09
LCB 200×75×20×1.0	6.85	5.34	6.36	1.28	1.08
LCB 200×75×20×1.5	13.78	10.92	12.58	1.26	1.10
LCB 200×75×20×2.0	23.26	17.75	20.12	1.31	1.16
Mean				1.28	1.14
COV				0.024	0.043

387

388   The parametric study results of FE simulations of three-point loading setup for $a/d_1=1.0$
389   (Scenario 2 in Table 6) are summarised in Table 9 while Tables 10-13 provide that of the
390   sections with longer spans (Scenario 3 in Table 6). In Tables 9-13, V and M are the numerical
391   values of the shear force and the bending moment at the failure of the section, respectively.
392    $V_{EC3,[19]}$ is the shear resistance of the section according to Eurocode 3 for stainless steel
393   calculated from Eq. (6) where modified expressions for shear buckling reduction factor from
394   [19] (using Table 2) were incorporated. $V_{DSM,\,[19]}$ is the DSM shear capacity of the section
395   calculated from Eqs. (12)-(14).

396   The mean and the COV of FE to predicted shear capacity ratio given in Table 9 suggest that
397   the numerical shear capacities are agree well with the shear capacity predictions. Therefore,

20

398   this confirms that the shear capacity of the section is not affected by the bending moment when

399   shorter spans (a/d_1=1.0) are employed. In addition, the bending moment of the section (M) is

400   compared with the bending resistance consisting of the effective flange area ($M_{f,Rd}$) in Table 9.

401   This comparison suggests that even though the section moment (M) is as high as $1.3 \times M_{f,Rd}$, the

402   shear capacity (V) of the section is not reduced.

403   Further, the progressive reduction of the section shear force (V) compared to the section shear

404   resistance is observed with the increment of the section bending moment (M) compared to the

405   section bending resistance from Tables 10-13. This confirms that the numerically obtained

406   shear capacities of the sections with longer spans are not independent of bending stresses of

407   the section. Therefore, the shear provisions given in Section 2 were utilised to calculate the

408   shear resistances of sections when evaluating the bending-shear interaction equations in

409   Section 6. However, no reduction in section bending moment (M) can be observed for sections

410   with aspect ratios of 3.0 and 5.0 from Tables 12 and 13.

411   Moreover, FE results shows that the employed duplex stainless steel grade results in higher

412   shear forces and bending moments in the sections than austenitic stainless steel grade.

413   However, no clear difference was observed in the interaction behaviour of the sections of these

414   two stainless steel grades from the numerical results of the parametric study.

415

416

417

418

419

420

421

422

423

424

21

Table 9 Numerical parametric study results of Scenario 2 (a/d_1=1.0)

LCB section	V (kN)	M (kNm)	$V_{EC3,[19]}$ (kN)	$V_{DSM,[19]}$ (kN)	$\dfrac{V}{V_{EC3,[19]}}$	$\dfrac{V}{V_{DSM,[19]}}$	$\dfrac{M}{M_{u,FE}}$	$\dfrac{M}{M_{f,Rd}}$
Stainless steel grade 1.4301								
LCB 150×65×15×1.0	15.25	2.27	14.27	13.89	1.07	1.10	0.74	1.28
LCB 150×65×15×1.5	27.62	4.10	25.91	25.55	1.07	1.08	0.71	1.18
LCB 150×65×15×2.0	40.15	5.94	38.66	38.53	1.04	1.04	0.74	1.19
LCB 200×75×20×1.0	17.23	3.43	16.24	15.82	1.06	1.09	0.80	1.38
LCB 200×75×20×1.5	32.19	6.39	30.42	29.65	1.06	1.09	0.73	1.27
LCB 200×75×20×2.0	48.90	9.68	46.25	45.59	1.06	1.07	0.76	1.21
Stainless steel grade 1.4462								
LCB 150×65×15×1.0	25.69	3.83	24.79	24.22	1.04	1.06	0.77	1.37
LCB 150×65×15×1.5	50.58	7.51	46.82	45.56	1.08	1.11	0.75	1.30
LCB 150×65×15×2.0	76.38	11.30	71.57	70.28	1.07	1.09	0.74	1.21
LCB 200×75×20×1.0	28.21	5.61	27.44	27.29	1.03	1.03	0.82	1.47
LCB 200×75×20×1.5	57.15	11.34	53.40	51.99	1.07	1.10	0.82	1.39
LCB 200×75×20×2.0	88.82	17.59	83.51	81.25	1.06	1.09	0.76	1.30
Mean					1.06	1.08	0.76	1.30
COV					0.015	0.022	0.046	0.070

434   Table 10 Numerical parametric study results of Scenario 3 (a/d₁=1.5)

LCB section	V (kN)	M (kNm)	$V_{EC3,[19]}$ (kN)	$V_{DSM,[19]}$ (kN)	$\frac{V}{V_{EC3,[19]}}$	$\frac{V}{V_{DSM,[19]}}$	$\frac{M}{M_{u,FE}}$
Stainless steel grade 1.4301							
LCB 150×65×15×1.0	12.07	2.70	13.25	13.32	0.91	0.91	0.88
LCB 150×65×15×1.5	22.49	5.01	24.39	24.63	0.92	0.91	0.87
LCB 150×65×15×2.0	33.01	7.33	36.61	37.34	0.90	0.88	0.91
LCB 200×75×20×1.0	13.34	3.98	14.93	15.14	0.89	0.88	0.93
LCB 200×75×20×1.5	26.19	7.80	28.34	28.48	0.92	0.92	0.89
LCB 200×75×20×2.0	39.69	11.79	43.52	43.94	0.91	0.90	0.92
Stainless steel grade 1.4462							
LCB 150×65×15×1.0	19.18	4.29	22.73	23.16	0.84	0.83	0.86
LCB 150×65×15×1.5	39.76	8.86	43.50	43.71	0.91	0.91	0.88
LCB 150×65×15×2.0	62.30	13.83	67.16	67.66	0.93	0.92	0.91
LCB 200×75×20×1.0	20.89	6.24	24.93	26.05	0.84	0.80	0.91
LCB 200×75×20×1.5	43.73	13.02	49.12	49.75	0.89	0.88	0.94
LCB 200×75×20×2.0	71.84	21.34	77.57	77.95	0.93	0.92	0.92
Mean					0.90	0.89	0.90
COV					0.034	0.043	0.027

435

436

437

438

439

440

441

442

443   Table 11 Numerical parametric study results of Scenario 3 (a/d_1=2.0)

LCB section	V (kN)	M (kNm)	$V_{EC3,[19]}$ (kN)	$V_{DSM,[19]}$ (kN)	$\dfrac{V}{V_{EC3,[19]}}$	$\dfrac{V}{V_{DSM,[19]}}$	$\dfrac{M}{M_{u,FE}}$
Stainless steel grade 1.4301							
LCB 150×65×15×1.0	9.76	2.91	12.82	13.02	0.76	0.75	0.95
LCB 150×65×15×1.5	18.20	5.41	23.74	24.13	0.77	0.75	0.94
LCB 150×65×15×2.0	26.29	7.78	35.78	36.68	0.73	0.72	0.97
LCB 200×75×20×1.0	10.63	4.23	14.38	14.77	0.74	0.72	0.98
LCB 200×75×20×1.5	21.18	8.41	27.47	27.85	0.77	0.76	0.96
LCB 200×75×20×2.0	31.95	12.65	42.35	43.06	0.75	0.74	0.99
Stainless steel grade 1.4462							
LCB 150×65×15×1.0	15.26	4.55	21.87	22.60	0.70	0.68	0.91
LCB 150×65×15×1.5	32.27	9.58	42.10	42.72	0.77	0.76	0.95
LCB 150×65×15×2.0	50.04	14.81	65.28	66.25	0.77	0.76	0.97
LCB 200×75×20×1.0	16.32	6.50	23.91	25.39	0.68	0.64	0.95
LCB 200×75×20×1.5	34.73	13.79	47.34	48.56	0.73	0.72	1.00
LCB 200×75×20×2.0	58.15	23.03	75.06	76.19	0.77	0.76	0.99
Mean					0.75	0.73	0.96
COV					0.040	0.52	0.026

444

445

446

447

448

449

450

451

452   Table 12 Numerical parametric study results of Scenario 3 (a/d_1=3.0)

LCB section	V (kN)	M (kNm)	$V_{EC3,[19]}$ (kN)	$V_{DSM,[19]}$ (kN)	$\dfrac{V}{V_{EC3,[19]}}$	$\dfrac{V}{V_{DSM,[19]}}$	$\dfrac{M}{M_{u,FE}}$
Stainless steel grade 1.4301							
LCB 150×65×15×1.0	6.73	3.01	12.48	12.71	0.54	0.53	0.98
LCB 150×65×15×1.5	13.04	5.81	23.22	23.62	0.56	0.55	1.01
LCB 150×65×15×2.0	18.42	8.18	35.11	36.00	0.52	0.51	1.02
LCB 200×75×20×1.0	7.11	4.24	13.96	14.41	0.51	0.49	0.99
LCB 200×75×20×1.5	14.93	8.89	26.78	27.20	0.56	0.55	1.02
LCB 200×75×20×2.0	22.21	13.19	41.43	42.14	0.54	0.53	1.03
Stainless steel grade 1.4462							
LCB 150×65×15×1.0	10.18	4.55	21.20	22.03	0.48	0.46	0.91
LCB 150×65×15×1.5	22.01	9.81	41.00	41.72	0.54	0.53	0.97
LCB 150×65×15×2.0	35.39	15.71	63.78	64.80	0.55	0.55	1.03
LCB 200×75×20×1.0	10.81	6.45	23.12	24.73	0.47	0.44	0.94
LCB 200×75×20×1.5	23.33	13.89	45.95	47.36	0.51	0.49	1.01
LCB 200×75×20×2.0	40.17	23.86	73.10	74.39	0.55	0.54	1.03
Mean					0.53	0.51	1.00
COV					0.058	0.070	0.037

453

454

455

456

457

458

459

460

461 Table 13 Numerical parametric study results of Scenario 3 (a/d_1=5.0)

LCB section	V (kN)	M (kNm)	$V_{EC3,[19]}$ (kN)	$V_{DSM,[19]}$ (kN)	$\dfrac{V}{V_{EC3,[19]}}$	$\dfrac{V}{V_{DSM,[19]}}$	$\dfrac{M}{M_{u,FE}}$
Stainless steel grade 1.4301							
LCB 150×65×15×1.0	4.23	3.15	12.30	12.46	0.34	0.34	1.03
LCB 150×65×15×1.5	7.97	5.92	22.93	23.21	0.35	0.34	1.03
LCB 150×65×15×2.0	11.24	8.32	34.74	35.45	0.32	0.32	1.03
LCB 200×75×20×1.0	4.31	4.29	13.73	14.11	0.31	0.31	1.00
LCB 200×75×20×1.5	8.99	8.92	26.40	26.69	0.34	0.34	1.02
LCB 200×75×20×2.0	13.46	13.33	40.92	41.41	0.33	0.33	1.04
Stainless steel grade 1.4462							
LCB 150×65×15×1.0	6.16	4.59	20.84	21.57	0.30	0.29	0.92
LCB 150×65×15×1.5	13.65	10.14	40.40	40.91	0.34	0.33	1.01
LCB 150×65×15×2.0	21.68	16.04	62.96	63.64	0.34	0.34	1.05
LCB 200×75×20×1.0	6.64	6.61	22.69	24.20	0.29	0.27	0.96
LCB 200×75×20×1.5	13.87	13.77	45.20	46.40	0.31	0.30	1.00
LCB 200×75×20×2.0	24.20	23.96	72.02	72.96	0.34	0.33	1.03
Mean					0.33	0.32	1.01
COV					0.060	0.073	0.036

462

## 6 Results analysis

The insight into the bending and shear interaction of cold-formed stainless steel LCBs acquired from the numerical studies conducted in this paper was utilised in assessing the interaction equations discussed in Section 2 and the details are presented in this section.

6.1 Failure modes

Using the FE results obtained in the parametric study, an analysis of failure modes was conducted and the dominant failure modes of three-point loading simulations of stainless steel LCB sections for each aspect ratio were identified. Fig. 10 illustrates the identified dominant failure modes of stainless steel LCB sections together with their load-deflection curves for each

26

472   aspect ratio. From Fig. 10 (a), it can be clearly seen that the diagonal shear failure of both webs

473   of sections with an aspect ratio of 1.0, and can be concluded that these sections fail primarily

474   in shear, as it is expected. Figs. 10 (b) and (c) depict the dominant failure modes of sections

475   with aspect ratios of 1.5 and 2.0, respectively. It is observed that both local buckling failure of

476   the compression flange and diagonal shear failure of the webs occur in the sections with these

477   two aspect ratios. Therefore, the sections with aspect ratios of 1.5 and 2.0 are subjected to the

478   bending and shear interaction. Local buckling of the compression flange is visible from Figs.

479   10 (d) and (e) for the sections with aspect ratios of 3.0 and 5.0, respectively, and there is no

480   clear sign of any web shear failure. This observation leads to the conclusion that sections with

481   aspect ratios of 3.0 and 5.0 behave primarily in bending. In the next section, the bending-shear

482   interaction equations discussed in Section 2 were assessed, while giving due consideration to

483   the above findings from FE analysis conducted in this study.

27

(a) Aspect ratio=1.0

(b) Aspect ratio=1.5

(c) Aspect ratio=2.0

(d) Aspect ratio=3.0
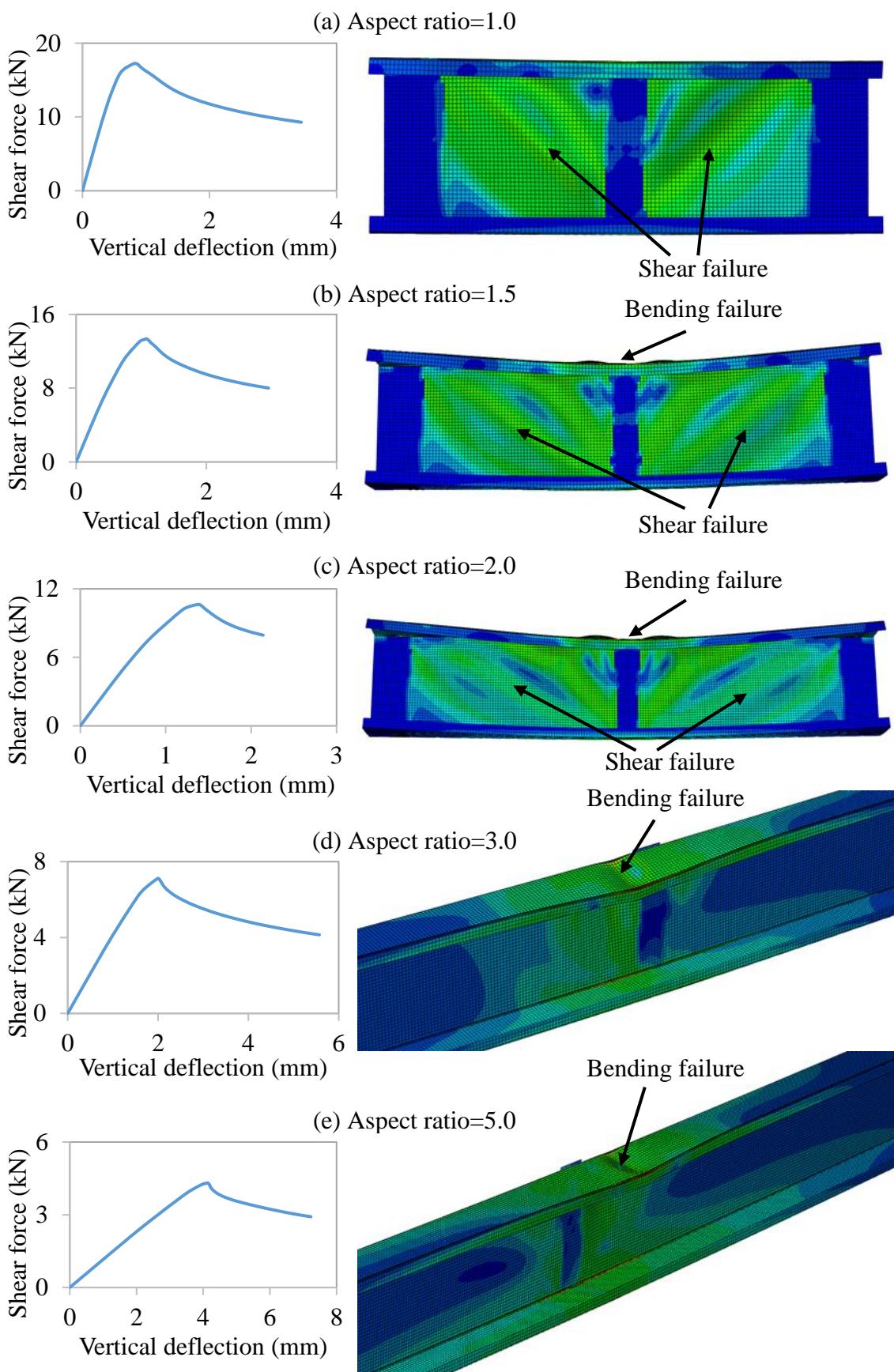
(e) Aspect ratio=5.0

484

485   Fig. 10 Failure modes and load-deflection curves of stainless steel LCB sections for different aspect ratios

28

486   6.2   Assessment of EN1993-1-3 interaction equation

487   The following sections are dealing with the evaluation of codified interaction equations for the

488   bending and shear interaction of cold-formed stainless steel LCB sections using the generated

489   numerical results of the parametric study. For this purpose, numerical resistance values were

490   compared with predicted resistance values. Fig. 11 illustrates the definition of the actual value

491   of the resistance (experimental or FE) with the predicted value of the resistance from an

492   interaction curve. The distance from the origin to the actual data point in the bending-shear

493   interaction diagram defines the actual resistance. The distance between the origin and the

494   intersection point of the origin to the actual data point line and the interaction curve represents

495   the predicted resistance. If the actual data point lies outside the interaction curve, it is said to

496   be a safe prediction and if the point lies within the curve it is said to be unsafe.
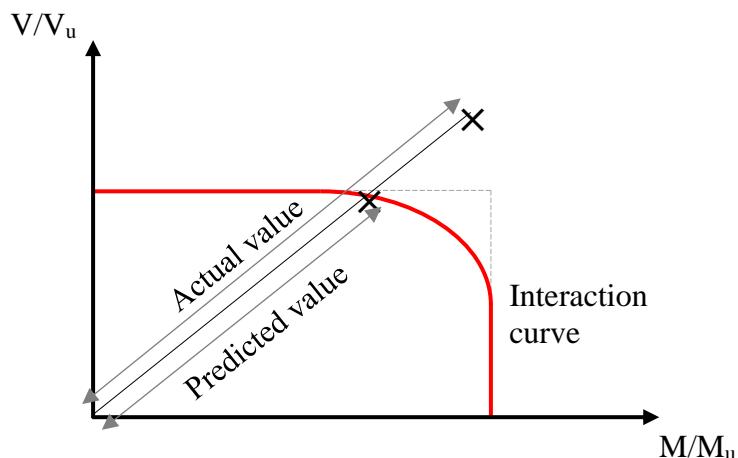

497

498   Fig. 11 Definition of actual and predicted resistances with respect to the interaction curve

499   Fig. 12 plots the FE results of stainless steel LCB sections given in Tables 9-13 for each aspect

500   ratio with the bending-shear interaction curve from EN1993-1-3 [12]. It can be observed from

501   the distribution of FE data points in the interaction diagram that LCB sections with an aspect

502   ratio of 1.0 do not exhibit any shear capacity reduction. However, a reduction of shear capacity

503   can be seen for the sections with aspect ratios of 1.5 and 2.0, when the bending and shear

504   interaction effect takes place. Also, there is no evidence of bending capacity reduction in the

505   sections with higher aspect ratios such as 3.0 and 5.0. From the comparison, it can be seen that

506   EN1993-1-3 [12] interaction equation is able to safely predict the resistance of cold-formed

507   stainless steel LCB sections subjected to bending and shear interaction, however, a

508   conservative nature in predictions may exist when $V/V_{w,Rd}$ ratio is closer to 1.0. This is because,

509   the assumption of bending-shear interaction when the applied bending moment (M) exceeds

the bending resistance of the flanges with effective flange area ($M_{f,Rd}$), seems to be not

applicable for cold-formed stainless steel LCB sections. It was shown that the shear capacity

of sections with shorter spans is not reduced even with a bending moment higher than $M_{f,Rd}$.

Therefore, modifications were applied to EN1993-1-3 [12] bending-shear interaction equation

with aiming to improve the predictions for cold-formed stainless steel LCBs, employing the

FE results. It can be also observed that there are two specimens with relatively different

behaviour in each set of data corresponding to longer spans, and these specimens are found to

be 1 mm thick sections of duplex stainless steel grade 1.4462. This makes these sections the

most slender specimens among the considered sections as they have the lowest thickness value

of 1 mm and the highest yield stress value of 500 MPa among the considered parameters.

Therefore, the influence of local buckling effects could be the reason for relatively lower

resistances in these slender sections.
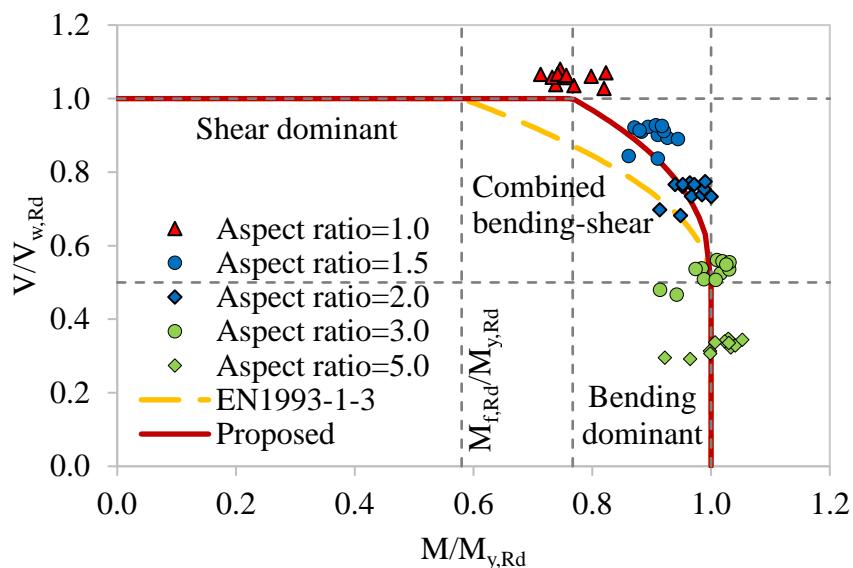
Fig. 12 FE results of stainless steel LCB sections with different aspect ratios against the current and proposed
EN1993-1-3 [12] interaction curves

Following the distribution of FE data points and taking into account the effect of bending-shear

interaction of LCB sections with aspect ratios of 1.5 and 2.0, EN1993-1-3 [12] interaction

equation was modified to the version shown in Eq. (18). When compared to the codified

version, the plastic bending resistance of the section ($M_{pl,Rd}$) is replaced with the bending

resistance of the section ($M_{y,Rd}$) in this proposed interaction equation and the exponent 2.35 is

employed instead of the exponent 2 to redefine the shape of the curve in the bending-shear

interaction region. An additional coefficient of 1.3 is introduced to the term bending resistance

30

532   consisting of the effective flange area ($M_{f,Rd}$), considering the higher bending moments

533   observed in LCB sections with shorter spans, to redefine the starting point of the bending-shear

534   interaction region.

535     $$\frac{M_{y,Ed}}{M_{y,Rd}} + \left(1 - \frac{1.3\,M_{f,Rd}}{M_{y,Rd}}\right)\left(\frac{2V_{Ed}}{V_{w,Rd}} - 1\right)^{2.35} \leq 1.0 \qquad (18)$$

536   The comparison of the numerical results with the proposed interaction curve is also shown in

537   Fig. 12. From Fig. 12, it can be seen that there is no reduction in the shear resistance ($V_{w,Rd}$)

538   up to a point closer to the sections with an aspect ratio of 1.0 in the proposed curve. Then, the

539   new curve takes into account the bending and shear interaction of cold-formed stainless steel

540   LCBs up to the location of the sections with an aspect ratio of 3.0 and follows a region of no

541   reduction in cross-section bending resistance ($M_{y,Rd}$). The proposed curve treats the interaction

542   with a curvature and follows well the numerical data points.

543   Then, a statistical evaluation was conducted for both codified and proposed interaction

544   equations. Tables 14 and 15 present the evaluation results calculated according to Fig. 11 for

545   codified and proposed interaction equations, respectively. The mean and the COV of each case

546   are also given in Tables 14 and 15. Table 14 comprises the sections with aspect ratios of 1.0,

547   1.5, and 2.0 as these are treated under bending-shear interaction in EN1993-1-3 [12] provisions.

548   However, only the values corresponding to aspect ratios of 1.5 and 2.0 are considered in Table

549   15 as only these two aspect ratios fall within the proposed interaction region.

550   Overall, the mean and the COV of numerical to predicted ratio are 1.17 and 0.096, respectively

551   for EN1993-1-3 [12] interaction equation while 1.03 and 0.032, respectively for the proposed

552   interaction equation. The reduced mean and COV of the proposed equation compared to the

553   codified interaction equation imply increased accuracy and consistency of predictions.

554

555

556

557

558

559

560   Table 14 Evaluation of EN1993-1-3 [12] interaction equation according to Fig. 11

LCB section	Aspect ratio=1.0	Aspect ratio=1.5	Aspect ratio=2.0
Stainless steel grade 1.4301			
LCB 150×65×15×1.0	1.28	1.16	1.06
LCB 150×65×15×1.5	1.16	1.12	1.04
LCB 150×65×15×2.0	1.12	1.12	1.04
LCB 200×75×20×1.0	1.40	1.22	1.09
LCB 200×75×20×1.5	1.23	1.18	1.08
LCB 200×75×20×2.0	1.20	1.16	1.08
Stainless steel grade 1.4462			
LCB 150×65×15×1.0	1.34	1.10	0.99
LCB 150×65×15×1.5	1.30	1.16	1.07
LCB 150×65×15×2.0	1.21	1.17	1.08
LCB 200×75×20×1.0	1.44	1.17	1.02
LCB 200×75×20×1.5	1.44	1.23	1.10
LCB 200×75×20×2.0	1.28	1.22	1.12
Mean	1.28	1.17	1.06
COV	0.082	0.036	0.033

561

562

563

564

565

566

567

568

569

570　　Table 15 Evaluation of proposed interaction equation for EN1993-1-3 [12] according to Fig. 11

LCB section	Aspect ratio=1.5	Aspect ratio=2.0
Stainless steel grade 1.4301		
LCB 150×65×15×1.0	1.04	1.01
LCB 150×65×15×1.5	1.01	0.99
LCB 150×65×15×2.0	1.03	1.00
LCB 200×75×20×1.0	1.07	1.03
LCB 200×75×20×1.5	1.06	1.02
LCB 200×75×20×2.0	1.04	1.03
Stainless steel grade 1.4462		
LCB 150×65×15×1.0	0.97	0.94
LCB 150×65×15×1.5	1.04	1.01
LCB 150×65×15×2.0	1.05	1.02
LCB 200×75×20×1.0	1.02	0.97
LCB 200×75×20×1.5	1.07	1.04
LCB 200×75×20×2.0	1.08	1.05
Mean	1.04	1.01
COV	0.029	0.029

571

572　6.3　Assessment of SEI/ASCE 8–02 interaction equation

573　SEI/ASCE 8–02 [17] bending-shear interaction equation for the sections with transverse
574　stiffeners was evaluated for cold-formed stainless steel LCB sections utilising the numerical
575　results generated in the parametric study and the assessment details are given in this section.
576　Fig. 13 compares SEI/ASCE 8–02 [17] interaction curve with the FE results from Tables 9-13.
577　From the comparison, it is apparent that the codified interaction equation is too conservative
578　when the V/V_n ratio is closer to 1.0. This is because SEI/ASCE 8–02 [17] interaction equation
579　treats the LCB sections with an aspect ratio of 1.0 within the bending-shear interaction region
580　as similar to EN1993-1-3 [12] interaction equation. Therefore, SEI/ASCE 8–02 [17] interaction
581　equation was modified considering the distribution of the numerical results.

582   Fig. 13 also includes the circular interaction equation given by Eq. (2) and the rounded

583   interaction equation given by Eq. (3). It can be concluded from the comparison that the circular

584   interaction equation is quite conservative for the bending-shear interaction of cold-formed

585   stainless steel LCB sections. This can be explained by considering the available post-buckling

586   resistance of the LCB sections, which is not taken into account in the circular interaction

587   equation. The rounded interaction equation given by Eq. (3) provides optimised predictions for

588   bending-shear interaction of cold-formed stainless steel LCBs. However, this is also found to

589   be conservative when the V/V_n ratio is closer to 1.0.
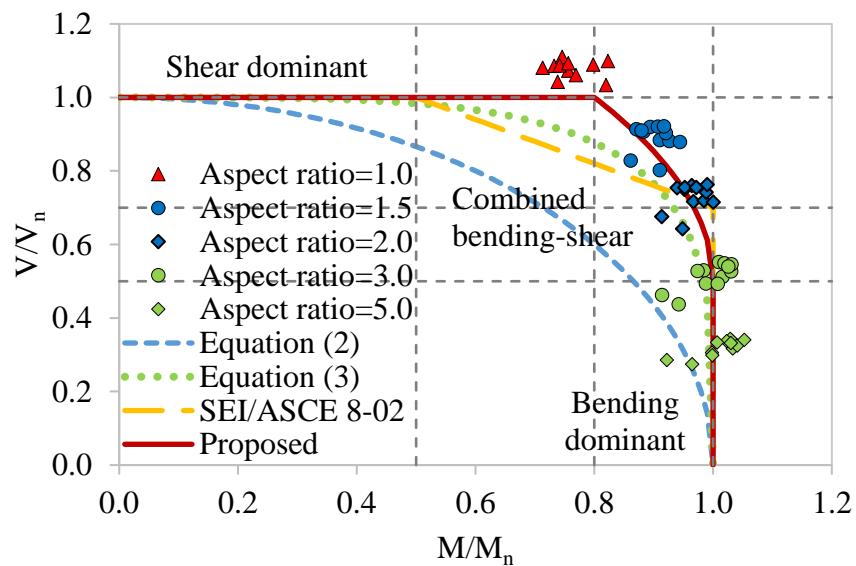
590

591   Fig. 13 FE results of stainless steel LCB sections with different aspect ratios against the current and proposed

592   SEI/ASCE 8–02 [17] interaction curves

593   Considering the bending and shear interaction effect of LCB sections with aspect ratios of 1.5

594   and 2.0, SEI/ASCE 8–02 [17] interaction equation was modified. The proposed interaction

595   equation for the bending and shear behaviour of cold-formed stainless steel LCB sections is

596   given by Eq. (19). This equation adopts a curved interaction as opposed to SEI/ASCE 8–02

597   [17] interaction equation and takes into account the bending-shear interaction when the applied

598   bending moment (M) exceeds 80 % of the bending capacity of the section (M_n) and when the

599   applied shear force (V) is greater than half of the section shear capacity (V_n).

600    $$\left(\frac{M}{M_n}\right) + 0.2\left(\frac{2V}{V_n} - 1\right)^2 \leq 1.0 \text{ for } \frac{M}{M_n} > 0.8 \text{ and } \frac{V}{V_n} > 0.5 \tag{19}$$

601 Fig. 13 illustrates the comparison of proposed interaction curve with the FE results. It is
602 observed from Fig. 13 that the proposed curve follows well the distribution of the numerical
603 results. Similar to the proposed EN1993-1-3 [12] curve, the proposed SEI/ASCE 8–02 [17]
604 interaction curve also treats the region between the FE data points corresponding to the sections
605 with aspect ratios of 1.0 and 3.0 for the bending-shear interaction of LCB sections.

606 Then, following a similar approach as discussed in Section 6.2, a statistical evaluation was
607 carried out for both codified and proposed SEI/ASCE 8–02 [17] interaction equations as well.
608 The evaluation results are given in Tables 16 and 17 for the codified and proposed interaction
609 equations, respectively with the mean and the COV of each case. Table 16 includes the results
610 of the sections with aspect ratios of 1.0, 1.5, and 2.0 while Table 17 provides the results for the
611 aspect ratios 1.5 and 2.0, as these fall within the bending-shear interaction regions of the
612 codified and proposed interaction curves, respectively.

613 From the evaluation, it was found that the codified interaction equation has an overall mean of
614 1.10 and an overall COV of 0.072 while that for the proposed interaction equation are 1.02 and
615 0.032, respectively. Therefore, relatively lower mean and COV suggest, improved accuracy
616 and consistency of predictions when using the proposed interaction equation.

617

618

619

620

621

622

623

624

625

626

627   Table 16 Evaluation of SEI/ASCE 8–02 [17] interaction equation according to Fig. 11

LCB section	Aspect ratio=1.0	Aspect ratio=1.5	Aspect ratio=2.0
Stainless steel grade 1.4301			
LCB 150×65×15×1.0	1.19	1.10	1.02
LCB 150×65×15×1.5	1.16	1.10	1.01
LCB 150×65×15×2.0	1.14	1.10	1.00
LCB 200×75×20×1.0	1.21	1.11	1.01
LCB 200×75×20×1.5	1.17	1.12	1.03
LCB 200×75×20×2.0	1.17	1.12	1.03
Stainless steel grade 1.4462			
LCB 150×65×15×1.0	1.17	1.03	0.94
LCB 150×65×15×1.5	1.20	1.11	1.02
LCB 150×65×15×2.0	1.18	1.13	1.03
LCB 200×75×20×1.0	1.17	1.04	0.93
LCB 200×75×20×1.5	1.23	1.11	1.01
LCB 200×75×20×2.0	1.19	1.13	1.04
Mean	1.18	1.10	1.01
COV	0.018	0.029	0.034

628

629

630

631

632

633

634

635

636

637   Table 17 Evaluation of proposed interaction equation for SEI/ASCE 8–02 [17] according to Fig. 11

LCB section	Aspect ratio=1.5	Aspect ratio=2.0
Stainless steel grade 1.4301		
LCB 150×65×15×1.0	1.01	1.00
LCB 150×65×15×1.5	1.01	0.99
LCB 150×65×15×2.0	1.03	1.00
LCB 200×75×20×1.0	1.04	1.02
LCB 200×75×20×1.5	1.04	1.02
LCB 200×75×20×2.0	1.05	1.04
Stainless steel grade 1.4462		
LCB 150×65×15×1.0	0.95	0.94
LCB 150×65×15×1.5	1.01	1.00
LCB 150×65×15×2.0	1.05	1.02
LCB 200×75×20×1.0	0.98	0.96
LCB 200×75×20×1.5	1.06	1.04
LCB 200×75×20×2.0	1.06	1.05
Mean	1.02	1.01
COV	0.033	0.031

638

6.4   Reliability analysis

640   The reliability assessment of the proposed interaction equations was carried out according to
641   Annex D of EN1990 [32] and SEI/ASCE 8-02 [17], and the details are summarised in this
642   section. The material and fabrication uncertainties were given due consideration in the analysis.
643   Afshan et al. [33] proposed statistical data for material parameters to use in reliability
644   calculations in a recent study and these values were adopted in the reliability calculations. The
645   material over-strength factor was taken as 1.3 and 1.1 for austenitic and duplex stainless steel
646   grades, respectively. The values of 0.06 and 0.03 were adopted for the COV of the material
647   strength. The COV of geometric properties was taken as 0.05. Table 18 summarises the key
648   parameters calculated according to EN1990 [32], Annex D to evaluate the reliability of the

649 proposed EN1993-1-3 [12] interaction equation where b is the mean value correction factor,

650 $k_{d,n}$ is the design fractile factor, V_δ is the coefficient of the variation of the error, and Υ_{M1} is the

651 partial safety factor. The calculated partial safety factor for the proposed interaction equation

652 is less than the recommended value of 1.1 in EN1993-1-4 [11]. The key parameters calculated

653 in the reliability analysis for SEI/ASCE 8-02 [17] are given in Table 19 where P_m and V_P are

654 the mean and the COV of the actual capacity to predicted capacity ratio, respectively, Ø is the

655 resistance factor, and β_0 is the target reliability index. The target reliability index was calculated

656 considering the data for each stainless steel grade separately. From the calculations, both values

657 for target reliability index are found to be greater than the recommended value of 3.0 for

658 structural members in SEI/ASCE 8-02 [17]. Therefore, the proposed interaction equations

659 satisfy the reliability requirements given in Annex D of EN1990 [32] and SEI/ASCE 8-02 [17].

660 Table 18 Summary of reliability analysis results calculated according to Annex D of EN1990 [32]

	No. of models	b	$k_{d,n}$	V_δ	Υ_{M1}
Proposed EN1993-1-3 interaction [12]	24	1.095	3.56	0.080	1.094

661

662 Table 19 Summary of reliability analysis results calculated according to SEI/ASCE 8-02 [17]

Stainless steel grade	No. of models	P_m	V_P	Ø	$\beta_0 > 3.0$
Austenitic	12	1.02	0.018	0.85	3.78
Duplex	12	1.01	0.043	0.85	3.02

663

7 Concluding remarks

665 This paper discusses the bending and shear interaction behaviour of cold-formed stainless steel

666 LCB sections which has been given less attention in the past. First, FE models were developed

667 and validated utilising the experimental results found from the literature for cold-formed

668 stainless steel and cold-formed steel. The validation included the comparison of ultimate loads,

669 failure modes and load-deflection curves of three-point and four-point loading tests, and the

670 FE results were found to be agreed well with the experimental results. Then, a comprehensive

671 numerical parametric study was conducted employing the validated FE models to extend the

672 database of cold-formed stainless steel LCBs considering different affecting parameters. This

673 study comprised 60 FE models of three-point loading simulations of stainless steel LCBs with
674 five different aspect ratios to investigate the shear and bending-shear interaction responses
675 while 12 FE models of four-point bending simulations of stainless steel LCBs to study the
676 bending response. Thereafter, the generated numerical database was analysed for the bending-
677 shear interaction of LCBs.

678 The diagonal web shear failure was observed in the sections with an aspect ratio of 1.0. Both
679 local buckling of the compression flanges and the diagonal web shear failure occurred in the
680 sections with aspect ratios of 1.5 and 2.0. The local buckling was taken place in the
681 compression flanges of the sections with higher aspect ratios of 3.0 and 5.0. Therefore, it was
682 concluded that the sections with aspect ratios of 1.5 and 2.0 are subjected to bending-shear
683 interaction.

684 Finally, Eurocode 3 and American specifications interaction equations were evaluated for the
685 bending-shear interaction of cold-formed stainless steel LCB sections using the FE results. It
686 was found that both EN1993-1-3 [12] and SEI/ASCE 8–02 [17] interaction equations are too
687 conservative for a higher level of applied shear force. This is because, the shear resistance of
688 stainless steel LCB sections with shorter spans is not reduced even with a bending moment as
689 high as $1.3 \times M_{f,Rd}$ and this is not taken into consideration in the codified treatment of bending-
690 shear interaction. Therefore, both interaction equations were revised and new interaction
691 equations were proposed using the FE results with aiming to enhance the prediction accuracy.
692 Further, a statistical evaluation was conducted for the proposed interaction equations and
693 assessment of those equations suggested improved and consistent predictions.

697 **References**

698 [1]   A. Olsson, Stainless steel plasticity-material modelling and structural applications, PhD
699   thesis, Lulea University of Technology, Sweden, 2001.
700 [2]   E. Real, E. Mirambell, I. Estrada, Shear response of stainless steel plate girders, Eng.
701   Struct. 29 (7) (2007) pp. 1626–1640.
702 [3]   N. Saliba, L. Gardner, Experimental study of the shear response of lean duplex stainless
703   steel plate girders, Eng. Struct. 46 (2013) pp. 375–391.

39

704 [4] X. W. Chen, H. X. Yuan, E. Real, X. X. Du, B. W. Schafer, Experimental behaviour of
705   stainless steel plate girders under combined bending and shear, J. Constr. Steel Res.
706   166 (2020).

707 [5] F. Sinur, D. Beg, Moment-shear interaction of stiffened plate girders - Tests and
708   numerical model verification, J. Constr. Steel Res. 85 (2013) pp. 116–129.

709 [6] F. Sinur, D. Beg, Moment-shear interaction of stiffened plate girders - Numerical study
710   and reliability analysis, J. Constr. Steel Res. 88 (2013) pp. 231–243.

711 [7] P. Keerthan, M. Mahendran, Experimental investigation and design of lipped channel
712   beams in shear, Thin-Walled Struct. 86 (2015) pp. 174–184.

713 [8] C. H. Pham, G. J. Hancock, Numerical simulation of high strength cold-formed purlins
714   in combined bending and shear, J. Constr. Steel Res. 66 (10) (2010) pp. 1205–1217.

715 [9] P. Keerthan, M. Mahendran, D. Hughes, Numerical studies and design of hollow flange
716   channel beams subject to combined bending and shear actions, Eng. Struct. 75 (2014)
717   pp. 197–212.

718 [10] K. Basler, Strength of plate girders under combined bending and shear, J. Struct. Div.
719   87 (7) (1961) pp. 181–197.

720 [11] EN 1993-1-4:2006+A1:2015, Eurocode 3 – Design of Steel Structures – Part 1–4:
721   General Rules – Supplementary Rules for Stainless Steels, European Committee for
722   Standardization (CEN), Brussels, 2015.

723 [12] EN 1993-1-3, Eurocode 3 – Design of steel structures – Part 1–3: General rules –
724   Supplementary rules for cold-formed members and sheeting, European Committee for
725   Standardization (CEN), Brussels, 2006.

726 [13] EN 1993-1-5, Eurocode 3 – Design of Steel Structures – Part 1–5: Plated Structural
727   Elements, European Committee for Standardization (CEN), Brussels, 2006.

728 [14] F. Bleich, Buckling Strength of Metal Structures, McGraw Hill, New York, USA, 1952.

729 [15] F. Shahabian, T. M. Roberts, Behaviour of plate girders subjected to combined bending
730   and shear loading, Scientia Iranica 15 (1) (2008) pp. 16–20.

731 [16] R. A. LaBoube, W. W. Yu, Cold-formed steel web elements under combined bending
732   and shear, Proceedings of the Fourth International Specialty Conference on Cold-
733   Formed Steel Structures, University of Missouri-Rolla, Missouri, USA, 1978, pp. 219–
734   251.

735 [17] SEI/ASCE 8–02, Specifications for the Design of Cold-Formed Stainless Steel
736   Structural Members, American Society of Civil Engineers (ASCE), Reston, 2002.

737 [18] T. Höglund, Behaviour and strength of the web of thin plate I-girders, Bulletin No. 93
738 of the Division of Building Statics and Structural Engineering, The Royal Institute of
739 Technology, Stockholm, Sweden, 1971, pp. 13–30.

740 [19] D. M. M. P. Dissanayake, K. Poologanathan, S. Gunalan, K. D. Tsavdaridis, B.
741 Nagaratnam, K. S. Wanniarachchi, Numerical modelling and shear design rules of
742 stainless steel lipped channel sections, J. Constr. Steel Res. (2019) (In press).

743 [20] AISI S100–16, North American Specification for the Design of Cold-Formed Steel
744 Structural Members, American Iron and Steel Institute (AISI), Washington, 2016.

745 [21] P. Keerthan, M. Mahendran, Experimental studies on the shear behaviour and strength
746 of LiteSteel beams, Eng. Struct. 32 (10) (2010) pp. 3235–3247.

747 [22] P. Keerthan, M. Mahendran, Shear behaviour and strength of LiteSteel beams with web
748 openings, Adv. Struct. Eng. 15 (2) (2012) pp. 171–184.

749 [23] M. Mahendran, P. Keerthan, Experimental studies of the shear behavior and strength
750 of LiteSteel beams with stiffened web openings, Eng. Struct. 49 (2013) pp. 840–854.

751 [24] R. Siahaan, M. Mahendran, P. Keerthan, Section moment capacity tests of rivet
752 fastened rectangular hollow flange channel beams, J. Constr. Steel Res. 125 (2016) pp.
753 252–262.

754 [25] I. Arrayago, E. Real, L. Gardner, Description of stress-strain curves for stainless steel
755 alloys, Mater. Des. 87 (2015) pp. 540–552.

756 [26] S. Niu, K. J. R. Rasmussen, F. Fan, Distortional-global interaction buckling of stainless
757 steel C-beams: Part II - Numerical study and design, J. Constr. Steel Res. 96 (2014) pp.
758 40–53.

759 [27] P. Keerthan, M. Mahendran, New design rules for the shear strength of LiteSteel beams,
760 J. Constr. Steel Res. 67 (6) (2011) pp. 1050–1063.

761 [28] L. Gardner, D. A. Nethercot, Numerical modeling of stainless steel structural
762 components—A consistent approach, J. Struct. Eng. 130 (10) (2004) pp. 1586–1601.

763 [29] P. Keerthan, M. Mahendran, Numerical modeling of LiteSteel beams subject to shear,
764 J. Struct. Eng. 137 (12) (2011) pp. 1428–1439.

765 [30] P. Keerthan, M. Mahendran, Shear buckling characteristics of cold-formed steel
766 channel beams, Int. J. Steel Struct. 13 (3) (2013) pp. 385–399.

767 [31] P. Keerthan, M. Mahendran, Improved shear design rules of cold-formed steel beams,
768 Eng. Struct. 99 (2015) pp. 603–615.

769 [32] EN 1990:2002+A1:2005, Eurocode – Basis of Structural Design, European Committee
770 for Standardization (CEN), Brussels, 2005.

771   [33]   S. Afshan, P. Francis, N. R. Baddoo, L. Gardner, Reliability analysis of structural

772   stainless steel design provisions, J. Constr. Steel Res. 114 (2015) pp. 293–304.